

Article

Design of a Sky Camera-Based Cloud Monitoring Camera at the Agam Space and Atmospheric Observation Station, Bukit Kototabang

Article Info

Article history :

Received April 13, 2023
Revised May 20, 2023
Accepted May 30, 2023
Published September 30, 2023

Keywords :

Sky camera, fish eye, dome, sun filter

Syafrijon^{1*}, Fahmi Rahmatia², Ridho Pratama², Teguh Nugraha Pratama³, Ednofri², Muzirwan³, Ainaa Maya Munira binti Ismail⁴

¹Department of Electronics Engineering, Faculty of Engineering, Universitas Negeri Padang, Padang, Indonesia

²Agam Space and Atmospheric Observation Station, National Research and Innovation Agency (BRIN), Indonesia

³Center for Climate and Atmospheric Research, Earth and Maritime Research Organization, National Research and Innovation Agency (BRIN), Indonesia

⁴Mechanical Engineering Study Center, UiTM Johor Pasir Gudang Campus, Johor, Malaysia

Abstract. Indonesia is a center of convection and acts as a driving force for global atmospheric circulation due to its geographical position. Moreover, Kototabang Hill is one of the national strategic areas in the equatorial atmospheric observation room with limited cloud cover data so that tools and development are needed to meet these data needs. Sky Camera for the purpose of observing clouds (Cloud Camera) is urgently needed to complement the need for cloud cover data to support observation and research activities in the field of the atmosphere. The Cloud Camera design is done by modifying the CCD Camera with several supporting devices including fish eye, solar tracker, sun filter and dome. Evaluation of the urgency of these enhancements is discussed in this paper. Among the four combinations of using supporting instruments (dome and sun filter) for the Cloud Camera device, the best image obtained is the device that uses a sun filter and without a dome. Among the four combinations of using supporting instruments (dome and sun filter) for the Cloud Camera device, the best image obtained is the device that uses a sun filter and without a dome.

This is an open access article under the [CC-BY](https://creativecommons.org/licenses/by/4.0/) license.



This is an open access article distributed under the Creative Commons 4.0 Attribution License, which permits unrestricted use, distribution, and reproduction in any medium, provided the original work is properly cited. ©2023 by author.

Corresponding Author :

Syafrijon

Department of Electronics Engineering, Faculty of Engineering, Universitas Negeri Padang, Indonesia

Email : syafrijon@ft.unp.ac.id**1. Introduction**

Indonesia, geographically located on the equator between two continents and two oceans. This condition makes Indonesia a center of convection and acts as a driving force for global atmospheric circulation. The island of Sumatra has unique climatic characteristics both locally and regionally. This is because the area has mountains that stretch from north to south and is surrounded by the Indian Ocean, the Malacca Strait, the Java Sea, the Karimata Strait and is close to the South China Sea. So that the formation of clouds and rain in Indonesia, especially Sumatra, are not only influenced by air circulation on a global and regional scale, they are also influenced by local conditions. Local influences such as topography make the variability of rainfall even greater due to the formation and cloud cover in the area.

Kototabang Hill is one of the national strategic areas in the equatorial atmosphere observation space. Located at an altitude of 865 meters above sea level, and coordinates 0.2°S; 100.32°E, this area is unique in terms of position and topography. The western part of Kototabang Hill is a coastal area directly facing the Indian Ocean, and in the eastern part is a highland area dominated by Bukit Barisan. This unique characteristic is also reflected in the two peaks of rain in one year on Kototabang Hill.

The movement of clouds in Kototabang has its own level of complexity. This is due to its position in the western part of Indonesia which experiences events such as trade winds and moonson winds whose effects are not even so defined for that area. The relationship between rain and clouds makes both of them very interesting to discuss. Observation and understanding of cloud patterns will be needed for many things, one of which is related to rainfall and its predictions.

Research on extreme rain conditions in Padang, West Sumatra on February 14 2018 used atmospheric data, including cloud cover data. Unfortunately the availability of cloud cover data from observation equipment is lacking. Sky Camera is an instrument in the form of an imager that is used to observe sky conditions, in this case it is more specifically used for observing clouds. By using a modified CCD camera, the complement is a fish eye, dome, solar tracker and sun filter [1-2]. The Sky Camera, which is generally available today, is only to get an image of the sky without a sun filter which makes the resulting image too dazzling around the sun area [3-4]. With the sun filter connected to the solar tracker, it is hoped that glare around the sun area can be avoided while at the same time we can make sun observations such as giant sunspots and solar eclipse phases. While the dome is used as a protective device that will certainly be used outdoors [5-7].

Sky Camera can provide real visualization of atmospheric conditions which will be very much needed, especially during extreme conditions. Thus helping researchers get a clearer picture of atmospheric conditions that have been observed by other atmospheric observation equipment. In this paper, we will also examine the urgency of the supporting instruments in the form of domes and solar filters used [8-10].

2. Experimental Section**2.1. Materials**

The design and development of the Sky Camera for cloud observation (Cloud Camera) is an engineering activity by modifying a CCD camera with a fish eye and a solar tracker and connected to a PC [11]. Then it is equipped with an additional solar tracker and sun filter to cover glare and reflections from direct sunlight so that the resulting image is expected to be more accurate [12]. The

results from the camera will be processed on a PC using software to perform image processing to produce cloud cover percentage data [13].

The main instrument used is a CCD camera which is supported by several other devices such as a fish eye, solar tracker, sun filter and dome (Figure 1). The camera used is ZWO ASI 178mc with IMX178 CMOS sensor specifications, sensor size 1/1.8 inch (7.4mm x 5mm), Effective resolution 6.4 megapixels (3096 x 2080), pixel size 2.4 μ m x 2.4 μ m, mono camera type (black and white) with bayer RGB filter, connectivity: USB 3.0, 14-bit dynamic range read rate up to 35 frames per second at full resolution, interface: ST-4 Guide Port. The ZWO ASI178MC camera is designed for astrophotography and is used primarily for shooting the night sky, imaging planets, the moon and other celestial objects [14]. With its high resolution and wide dynamic range, this camera is suitable for taking detailed astronomical images [15].

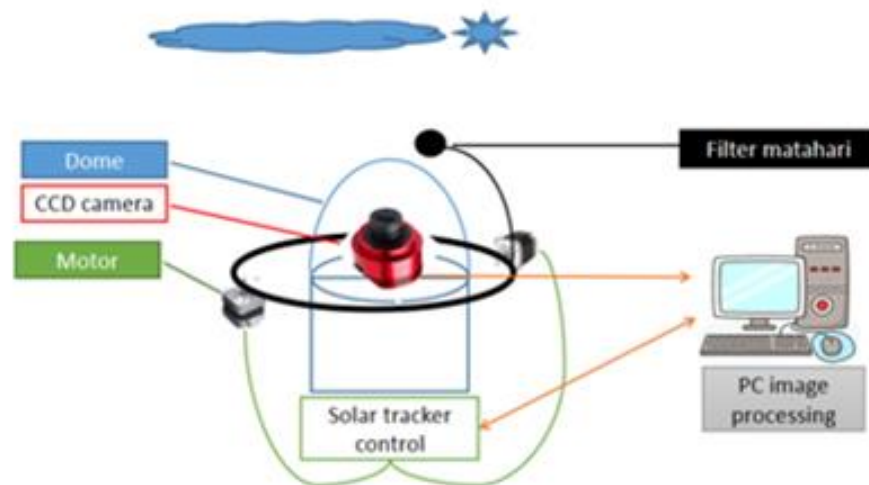


Figure 1. Block diagram of the basic system

The use of fish eye supports the camera to get an overview of the conditions of the entire sky with wide coverage. The solar tracker is used as a device that follows the daily movement of the sun using Arduino Uno, real time clock and MG90 servo motor [16-17]. The sun filter is expected to be able to block glare and reflections from the sun. Meanwhile, to protect the outside of the device which consists of a camera, filter, and servo motor, a dome is used [18]. Camera and solar tracker connect to PC to control solar tracker, save images and image processing [19].

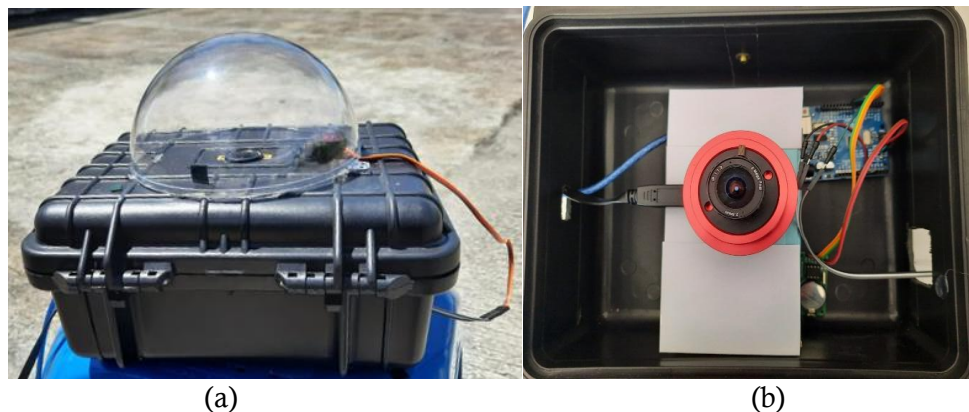


Figure 2. (a) Looks from outside the box; (b) seen from inside the box

2.2. Methods

The research methodology on the design and development of the Sky Camera for cloud observation (Cloud Camera) is an engineering activity by modifying a CCD camera with a fish eye and a solar tracker and connected to a PC. Then it is equipped with an additional solar tracker and sun filter to cover glare and reflections from direct sunlight so that the resulting image is expected to be more accurate [20]. The results from the camera will be processed on a PC using software to perform image processing to produce cloud cover percentage data [21].

2.2.1. System Flow Chart

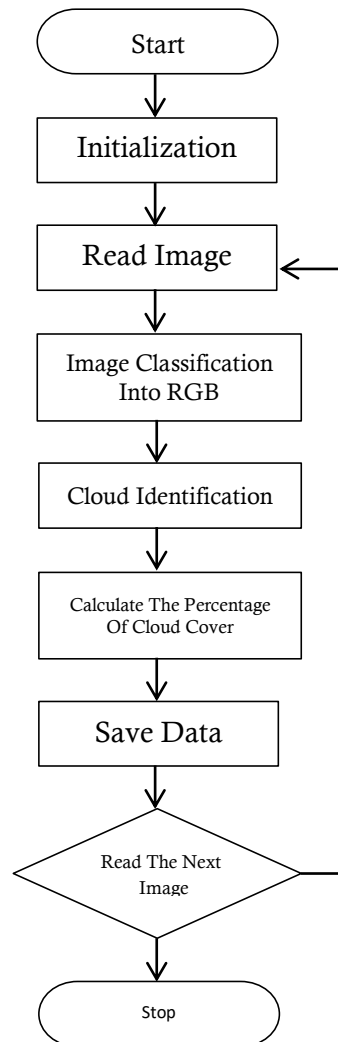


Figure 3. System flow chart

The software used consists of software for controlling CCD cameras and software for image data processing [22]. CCD camera control software is used to set the camera, data output, shooting range, camera resolution, shooting time range and shooting settings. Then software is used to process the resulting image data from the CCD camera [23]. To facilitate the making of this software design, a workflow diagram of the overall system is needed, shown in Figure 3. The flowchart begins with the program initialization process, then reads the captured images from the CCD camera. The image is then processed from image data to data in RGB format. Next identify each pixel as a cloud image or

not a cloud. Finally, the system performs large calculations of the percentage of cloud cover, cloud type identifiers and cloud movement directions.

2.2.2. Solar Tracker using Arduino Uno

The movement of the solar filter by a servo motor is controlled using an Arduino Uno. The system starts from reading the time in real time from the Real Time Clock (RTC) module [24]. The servo motor will go to the angle of the sun's position according to time and move 1° every 4 minutes following the daily movement of the sun. At night, the angular position of the servo motor returns to the zero position. This Arduino added a temperature sensor to monitor system temperature. In the development of this system and if further needed, slots are available for other sensors to be added.

2.2.3. Image Processing using Python

Color-based segmentation techniques, there are several other approaches that can be used for cloud and non-cloud image processing [25-26]. Here are some commonly used approaches:

- a. Texture Based Segmentation: can use texture features such as an orientation gradient histogram (HOG), Gabor filters, or other texture processing methods to differentiate between clouds and background.
- b. Segmentation Based on Geometry Features: can use geometric features such as shape, size, or spatial texture to separate clouds and background. Methods such as the Hough transform or contour analysis can be used in this regard.
- c. Machine Learning Algorithm Based Segmentation: can use machine learning based approaches such as classifiers such as Support Vector Machine (SVM), Random Forest, or Convolutional Neural Network (CNN) to identify and segregate clouds and background. This requires a well-annotated dataset to train the model [27].
- d. Advanced Image Processing Based Segmentation: Image processing methods such as compaction, smoothing, noise removal, or region based segmentation such as watershed algorithm or matrix based pixel separation can be used to separate clouds from the background [28].

The choice of technique depends on the complexity of the image and the desired accuracy. In some cases, a combination of techniques may also be required for better results [29]. For cloud and non-cloud image processing using Python, you can use various libraries or libraries such as OpenCV (Open Source Computer Vision Library) and NumPy [30]. The following is a simple example of how to process cloud imagery using Python importing the required library, reading cloud imagery, converting the image to a grayscale image, performing thresholding to separate cloud and background, displaying the processed image.

3. Results and Discussion

The Cloud Camera or Sky Camera device for cloud monitoring that is designed to be operated to get the first results at the office location of the Agam Space and Atmospheric Observation Station, Bukit Kototabang, Agam Regency, West Sumatra. Based on the geographical aspect, it is located in the equatorial region as a cloud producer which is quite high in the Sumatra region, so that the need for Cloud Camera data collection on the presence of clouds can be carried out properly. Data collection was carried out with several variations to review the urgency of additional devices used in basic cameras, namely domes and sun filters.

3.1. Image Processing

Image processing that has been carried out to determine clouds and non-clouds as well as the percentage of cloud cover with variations in the use of domes and sun filters can be an evaluator of the use of these instruments. Several processes and repetitions were carried out to get the best

processing script with better accuracy. Identification of clouds and non-clouds was carried out with several trials until the best constant was found.

3.1.1. Identify the Background

The picture taken is not completely sky. Backgrounds such as buildings and trees around are also captured by the camera [31]. The background needs to be separated from the cloud percentage calculation. From observing the captured images, it can be seen that backgrounds, especially natural backgrounds such as trees and hills, generally have relatively lower/dimmer R, G and B values [32]. For this reason, the authors are looking for the best limit value so that lower values can be identified as background and higher values are identified as non-background [33].

The image below shows a processing comparison where the limit values are 20, 30, and 40. At a limit value of 20, it is found that there are still relatively many background pixels in the image in the form of trees and buildings that fail to be identified as a background [34-35]. At a limit value of 40 there are some sky pixels that are identified as background, when in fact they are not. So based on that, the selected limit value at is 30. Any pixel with R,G and B values respectively smaller than 30, will be identified as background [36-37].

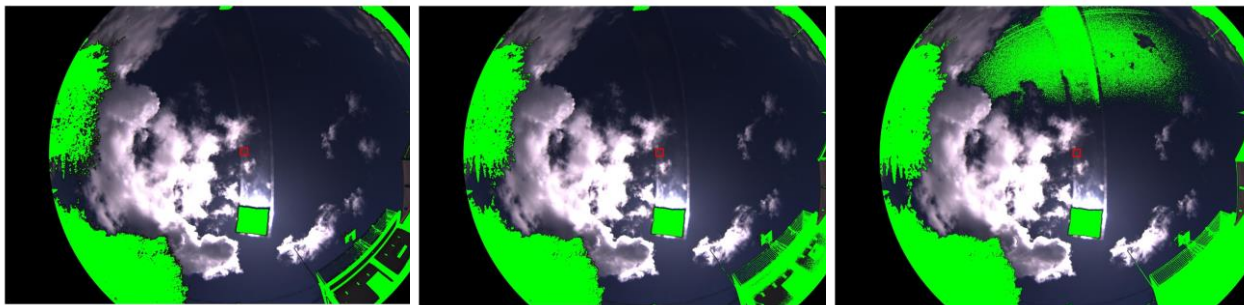


Figure 4. Processing comparisons where the cutoff values are 20, 30, and 40

3.1.2. Sun Identification

Sun and cloud pixels have similarities in that they can be both white. To overcome this, pixels with white values (255,255,255) will be given special treatment. The script that is created and used for this still has drawbacks because it is not equipped with data on the sun's position [38]. Hence for the purposes of this processing, the position of the sun was determined manually. From the value of the sun's position obtained, it will be determined whether the white pixel is the sun or a cloud. If the white pixel is near where the sun should be, the pixel will be identified as the sun. If the white pixel is far from that position, or in other words, it's impossible for the sun to be in that position, then the white pixel will be known as a cloud.

3.1.3. Identify the Clouds against the Sky

After identifying the other components/noise in the form of background and sun, what remains in the image is the main component in the form of sky and clouds. The sky will be identified as a blue pixel in the image because the observations were made during the day. There are two methods/formulas that can be used to determine what kind of pixels will be categorized as "blue" or sky in an image. The first method uses the difference between the value of B and the value of R and G, where B has a greater value. Both can also use the ratio between the value of B to R and G, where B is also of greater value. B is larger than R and G, indicating a bluer pixel in the image. The alternative to be used is to use a combination of both [39-40].

Formula 1. Difference = $B - ((R+G) / 2)$

Formula 2. Ratio = $((B/ R) + (B/G)) / 2$

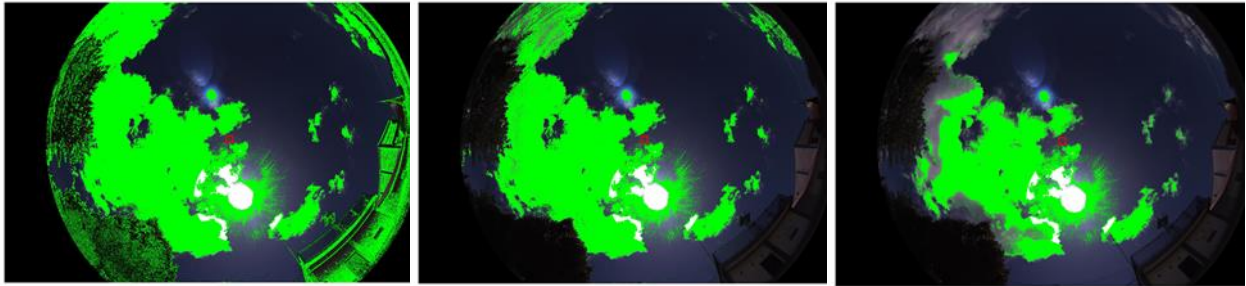


Figure 5. Differences in processing results with values $s=0$, $s=10$, $s=20$.

It can be seen that when using the criterion $s=0$, many background pixels are identified as clouds, whereas when $s=20$, many cloud pixels fail to be identified. The following figure shows the difference in processing results with the values $r=1.15$, $r=1.25$ and $r=1.35$.

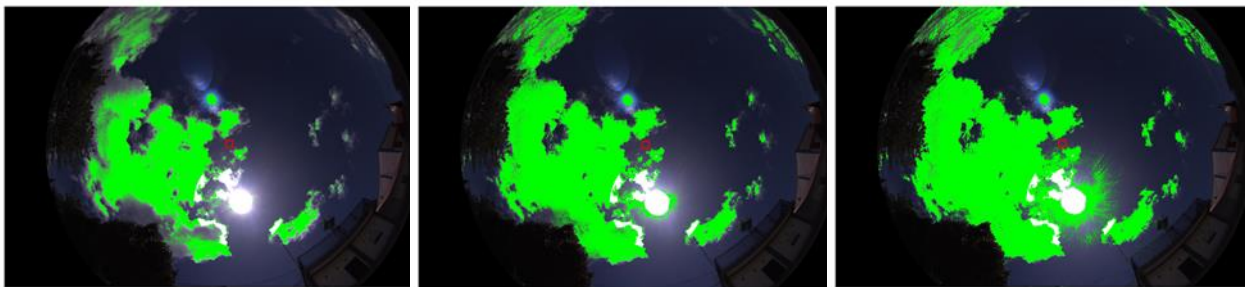


Figure 6. Differences in processing results with values $r=1.15$, $r=1.25$ and $r=1.35$.

Value 00068 with $r=1.15$, $r=1.25$ and $r=1.35$ from processing with a value of $r=1.15$ there are some cloud pixels near the horizon that are not identified. In processing using $r=1.35$, many of the luminescence areas around the sun are identified as clouds, even though they are just solar luminescence. Therefore, the median value of 1.25 is taken to accommodate this. From the differences in processing results using these different constants, the blue/sky color in the image is decided if the ratio between B to R and G is greater than 1.25. and the difference between B and R and G is greater than 10. The opposite value will be identified as a cloud. Furthermore, to calculate the percentage of cloud cover, it is calculated by the ratio between the cloud pixels and the total pixels in the image minus the number of background pixels.

Formula 3. (cloud percentage) = $(\text{cloud pixel count}) / ((\text{total pixel count}) - (\text{background pixel count})) \times 100\%$

Figure 4 shows the processed images of (a) a device without a dome and without a sun filter, (b) a device using a dome without a sun filter, (c) a device without a dome and using a sun filter, and (d) a device using a dome and a sun filter.

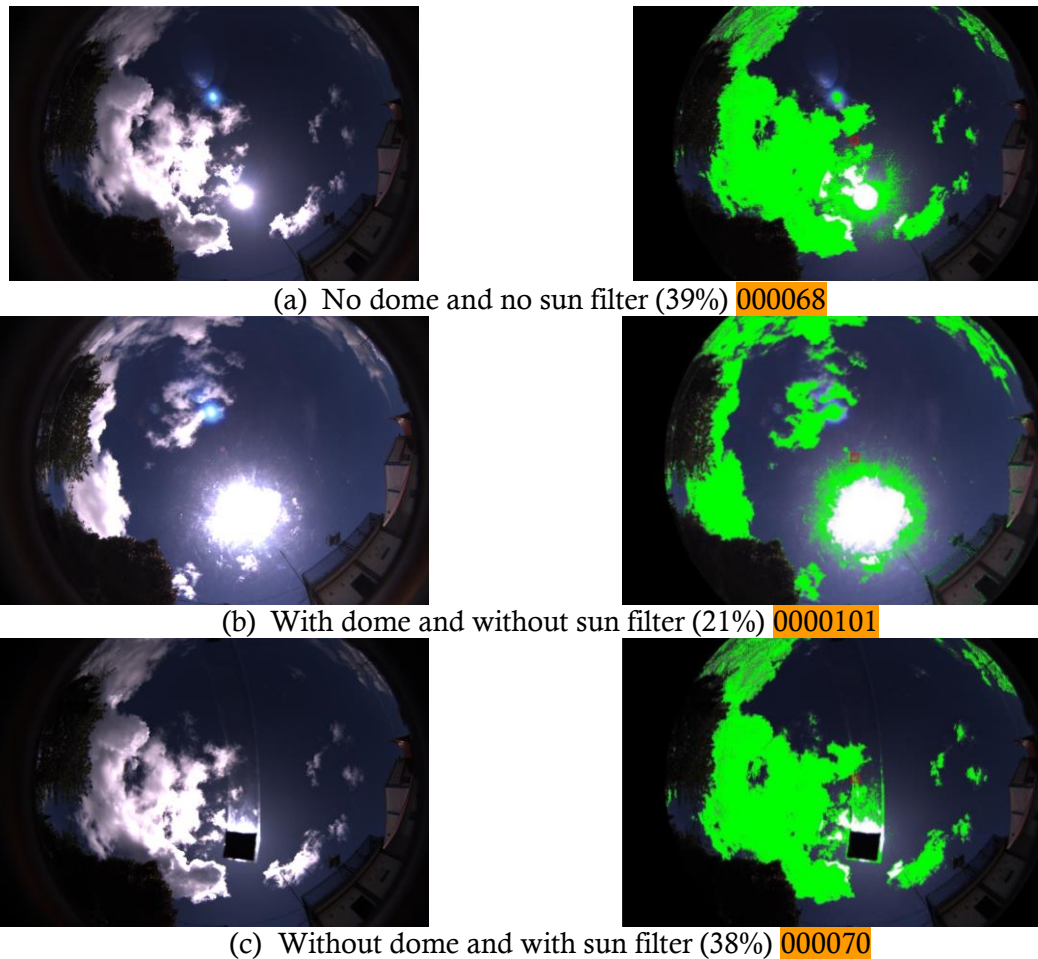


Figure 7. Comparison of Cloud Camera image results; RAW image (left; green color shows clouds) with dome and variations sun filter as well as cloud cover percentage display

3.2. Effect of Dome on Data Results

The effect of using a sun filter on the Cloud Camera device can be seen from the scattering of sun glare (flares) marked with purple boxes in Figure 4 (a) and (b) processed. The flare looks reduced or even disappears and the glow around the sun is also reduced when the sun filter is used (Figure 4(d)). While the use of a dome which actually plays an important role as a protective device used outdoors for quite a long time actually adds glow around the sun and increases the visual area of the sun. Comparing Figure 4 (a) and (b) processing, the yellow box shows the luminescence of the area around the sun which is quite extensive and is detected as a cloud with Figure 4 (c) and (d) without a dome with clearer image results.

There is an evaluation of the use of filters for data reading, namely flares and luminescence around the sun are detected as clouds, with the presence of a sun filter, the analysis of data readings becomes more accurate. However, because the sun filter used is attached to a plastic plate as a moving medium, the plastic plate produces a dome-like effect even though the area is quite small. Based on Figure 4 after analysis, the best image obtained is obtained from a device that uses a sun filter and without a dome. However, due to the continuous operation of the Cloud Camera outdoors, a dome

will still be needed for camera security with a solution using another type of dome which might reduce the widespread effect of sunlight.

4. Conclusion

Image processing that has been carried out to determine clouds and non-clouds as well as the percentage of cloud cover with variations in the use of domes and sun filters can be an evaluator of the use of these instruments. There is an evaluation of the use of filters for reading data, namely flares and glow around the sun are detected as clouds, with a solar filter, the analysis of data readings becomes more accurate. However, because the sun filter used is attached to a plastic plate as a moving medium, the plastic plate produces a dome-like effect even though the area is quite small.

5. Acknowledgements

We also appreciate the full support from DR. Tech Marzuki and lecturers at the Department of Physics, University of Andalas for the input provided in the implementation of the Sky Camera-Based Cloud Monitoring Camera Design at the Agam Space and Atmospheric Observation Station, Bukit Kototabang.

References

- [1] O. El Alani, M. Abraim, H. Ghennioui, A. Ghennioui, I. Ikenbi, and F. E. Dahr. (2021). Short term solar irradiance forecasting using sky images based on a hybrid CNN–MLP model, *Energy Reports*, vol. 7, no. May, pp. 888–900.
- [2] Caldas, M., & Alonso-Suárez, R. (2019). Very short-term solar irradiance forecast using all-sky imaging and real-time irradiance measurements. *Renewable energy*, 143, 1643-1658.
- [3] Z. Kolláth, A. Cool, A. Jechow, K. Kolláth, D. Száz, and K. P. Tong. (2020). Introducing the dark sky unit for multi-spectral measurement of the night sky quality with commercial digital cameras, *J. Quant. Spectrosc. Radiat. Transf.*, vol. 253.
- [4] Jechow, A., Kyba, C. C., & Hölker, F. (2019). Beyond all-sky: assessing ecological light pollution using multi-spectral full-sphere fisheye lens imaging. *Journal of Imaging*, 5(4), 46.
- [5] L. W. Hung, S. J. Anderson, A. Pipkin, and K. Fristrup. (2021). Changes in night sky brightness after a countywide LED retrofit, *J. Environ. Manage.*, vol. 292, no. May, p. 112776.
- [6] Robles, J., Zamorano, J., Pascual, S., Sánchez de Miguel, A., Gallego, J., & Gaston, K. J. (2021). Evolution of brightness and color of the night sky in Madrid. *Remote Sensing*, 13(8), 1511.
- [7] Hung, L., Anderson, S., Pipkin, A., Meadows, B., & Fristrup, K. (2020, January). Changes in night sky brightness after a countywide LED lighting retrofit. In *American Astronomical Society Meeting Abstracts# 235* (Vol. 235, pp. 378-02).
- [8] A. Saveliev, V. Izhboldina, M. Letenkov, E. Aksamentov, and I. Vatamaniuk. (2020). Method for automated generation of road accident scene sketch based on data from mobile device camera, *Transp. Res. Procedia*, vol. 50, no. 2019, pp. 608–613.
- [9] Thompson, A. P., Swiler, L. P., Trott, C. R., Foiles, S. M., & Tucker, G. J. (2015). Spectral neighbor analysis method for automated generation of quantum-accurate interatomic potentials. *Journal of Computational Physics*, 285, 316-330.
- [10] Pintore, G., Garro, V., Ganovelli, F., Gobbetti, E., & Agus, M. (2016). Omnidirectional image capture on mobile devices for fast automatic generation of 2.5 D indoor maps. In *2016 IEEE winter conference on applications of computer vision (WACV)* (pp. 1-9). IEEE.
- [11] G. Terrén-Serrano, A. Bashir, T. Estrada, and M. Martínez-Ramón. (2021). Girasol, a sky imaging and global solar irradiance dataset, *Data Br.*, vol. 35, pp. 1–12.
- [12] Z. Xu *et al.*, (2022). Pavement crack detection from CCD images with a locally enhanced transformer network, *Int. J. Appl. Earth Obs. Geoinf.*, vol. 110, no. May, p. 102825.

-
- [13] V. E. Savanevych *et al.*, (2022). CoLiTecVS software for the automated reduction of photometric observations in CCD-frames, *Astron. Comput.*, vol. 40, p. 100605.
- [14] K. F. Cho, N. Javier, and K. Choi. (2022). BRET measurement on CCD camera-based microtiter plate readers, *SLAS Discov.*, vol. 27, no. 7, pp. 413–417.
- [15] P. S. Minz and C. S. Saini. (2021). RGB camera-based image technique for color measurement of flavored milk, *Meas. Food*, vol. 4, no. July, p. 100012.
- [16] A. Gkiolmas, C. Dimakos, A. Chalkidis, and A. Stoumpa. (2020). An environmental education project that measures particulate matter via an Arduino interface, *Sustain. Futur.*, vol. 2, no. February, p. 100027.
- [17] W. Vallejo, C. Diaz-Uribe, and C. Fajardo. (2020). Do-it-yourself methodology for calorimeter construction based in Arduino data acquisition device for introductory chemical laboratories, *Heliyon*, vol. 6, no. 3, p. e03591.
- [18] J. S. Han *et al.* (2021). Decoupled error dynamics design for discrete-time sliding mode control in industrial servo systems under control input saturation and disturbance, *Mechatronics*, vol. 77, p. 102581.
- [19] N. La Forgia, E. H. Herø, and H. A. Jakobsen. (2021). High-speed image processing of fluid particle breakage in turbulent flow, *Chem. Eng. Sci. X*, vol. 12, p. 100117.
- [20] K. Jaskolka, J. Seiler, F. Beyer, and A. Kaup. (2019). A Python-based laboratory course for image and video signal processing on embedded systems, *Heliyon*, vol. 5, no. 10.
- [21] W. Chen, W. Wang, K. Wang, Z. Li, H. Li, and S. Liu. (2020). Lane departure warning systems and lane line detection methods based on image processing and semantic segmentation: A review, *J. Traffic Transp. Eng.*, vol. 7, no. 6, pp. 748–774.
- [22] A. Nasirahmadi *et al.* (2019). Automatic scoring of lateral and sternal lying posture in grouped pigs using image processing and Support Vector Machine, *Comput. Electron. Agric.*, vol. 156, no. September 2018, pp. 475–481
- [23] H. Safari, B. J. Balcom, and A. Afrough. (2021). Characterization of pore and grain size distributions in porous geological samples – An image processing workflow, *Comput. Geosci.*, vol. 156, no. March, p. 104895.
- [24] O. Debauche, S. Mahmoudi, S. A. Mahmoudi, P. Manneback, J. Bindelle, and F. Lebeau. (2019). Edge computing and artificial intelligence for real-time poultry monitoring, *Procedia Comput. Sci.*, vol. 175.
- [25] F. Ortin and J. Escalada. (2021). Cnerator: A Python application for the controlled stochastic generation of standard C source code, *SoftwareX*, vol. 15, p. 100711.
- [26] J. R. Terven and D. M. Córdova-Esparza. (2021). KinZ an Azure Kinect toolkit for Python and Matlab, *Sci. Comput. Program.*, vol. 211, p. 102702.
- [27] S. Xu and M. Zhang. (2022). Research on Credit Risk Assessment of Listed Companies in Technology Sector Based on Support Vector Machine Integration, *Procedia Comput. Sci.*, vol. 214, no. C, pp. 867–874.
- [28] N. Naval and J. M. Yusta. (2022). Comparative assessment of different solar tracking systems in the optimal management of PV-operated pumping stations, *Renew. Energy*, vol. 200, no. August, pp. 931–941.
- [29] B. Stanek, D. Węcel, Ł. Bartela, and S. Rulik. (2022). Solar tracker error impact on linear absorbers efficiency in parabolic trough collector – Optical and thermodynamic study, *Renew. Energy*, vol. 196, pp. 598–609.
- [30] C. Wang *et al.* (2022). Inversion of the refractive index of marine spilled oil using multi-angle sun glitter images acquired by the ASTER sensor, *Remote Sens. Environ.*, vol. 275, no. March p. 113019.
- [31] A. Rahdan, H. Bolandi, And M. Abedi. (2020). Design of on-board calibration methods for a
-

-
- digital sun sensor based on Levenberg–Marquardt algorithm and Kalman filters, *Chinese J. Aeronaut.*, vol. 33, no. 1, pp. 339–351.
- [32] S. Jiang, G. Shi, J. Cole-Dai, C. An, and B. Sun. (2021). Occurrence, latitudinal gradient and potential sources of perchlorate in the atmosphere across the hemispheres (31°N to 80°S), *Environ. Int.*, vol. 156, p. 106611.
- [33] E. Baumann *et al.* (2021). A backward-mode optical-resolution photoacoustic microscope for 3D imaging using a planar Fabry-Pérot sensor, *Photoacoustics*, vol. 24, no. March, p. 100293.
- [34] H. Ishiwata, N. Hasegawa, Y. Yonemaru, and K. Abe. (2022). A proposal of depth of focus equation for an optical system combined a digital image sensor, *Results Opt.*, vol. 6, p. 100182.
- [35] Cruz, Y. J., Rivas, M., Quiza, R., Beruvides, G., & Haber, R. E. (2020). Computer vision system for welding inspection of liquefied petroleum gas pressure vessels based on combined digital image processing and deep learning techniques. *Sensors*, 20(16), 4505.
- [36] X. Liu, D. Zhang, J. Liu, L. Wang, and S. Li. (2021). RGB Color Model Analysis for a Simple Structured Polydimethylsiloxane Pneumatic Micromixer, *SLAS Technol.*, vol. 26, no. 5, pp. 510–518.
- [37] Sarrafzadeh, M. H., La, H. J., Lee, J. Y., Cho, D. H., Shin, S. Y., Kim, W. J., & Oh, H. M. (2015). Microalgae biomass quantification by digital image processing and RGB color analysis. *Journal of applied phycology*, 27, 205-209.
- [38] L. Huang, B. Zhang, Z. Guo, Y. Xiao, Z. Cao, and J. Yuan. (2021). Survey on depth and RGB image-based 3D hand shape and pose estimation, *Virtual Real. Intell. Hardw.*, vol. 3, no. 3, pp. 207–234.
- [39] P. S. Minz and C. S. Saini. (2021). RGB camera-based image technique for color measurement of flavored milk, *Meas. Food*, vol. 4, no. October, p. 100012.
- [40] Nakano, K., Hirofuji, R., Ohnishi, T., Hauta-Kasari, M., Nishidate, I., & Haneishi, H. (2019). RGB camera-based imaging of oxygen saturation and hemoglobin concentration in ocular fundus. *IEEE Access*, 7, 56469-56479.